



# Crystal structure, thermal decomposition behavior, and fluorescence property of lanthanide complexes with 2,4,6-trimethylbenzoic acid

Xin-Xin Wang<sup>1</sup> · Jin-Jin Zhao<sup>1</sup> · Jian-Jun Zhang<sup>1</sup> · Ning Ren<sup>2</sup> · Shi-Kao Shi<sup>1</sup>

Received: 4 October 2021 / Accepted: 17 February 2022 / Published online: 10 March 2022  
© Akadémiai Kiadó, Budapest, Hungary 2022

## Abstract

Three new mononuclear lanthanide complexes  $[Ln(2,4,6\text{-TMBA})_3(\text{terpy})(\text{H}_2\text{O})]\cdot\text{C}_2\text{H}_5\text{OH}\cdot\text{H}_2\text{O}$  ( $Ln = \text{Gd}(1), \text{Er}(2)$  and  $[\text{Tb}(2,4,6\text{-TMBA})_3(\text{terpy})(\text{H}_2\text{O})]\cdot\text{C}_2\text{H}_5\text{OH}(3)$  (2,4,6-TMBA = 2,4,6-trimethylbenzoate, terpy = 2,2':6',2'-terpyridine) were synthesized by solution evaporation method with 2,4,6-trimethylbenzoic acid and 2,2':6',2'-terpyridine. These new lanthanide complexes were characterized by elemental analysis, infrared spectroscopy, single-crystal X-ray diffraction, and thermal analysis. The title complexes were found to be mononuclear units with the same coordination number of nine. The structures of the three lanthanide complexes could be divided into two types. The difference was that there were not only free ethanol molecules but also free water molecules in complexes 1–2, while there were only free ethanol molecules in complex 3. Thermogravimetry (TG), differential thermogravimetric (DTG), differential scanning calorimetry (DSC), and Fourier transform infrared spectroscopy (FTIR) were used to study the thermal behavior of complexes and the gas escaping from the thermal decomposition process. In addition, the fluorescence test showed that complex 3 had strong green luminescence properties, and the fluorescence lifetime of complex 3 was 0.637 ms.

**Keywords** Lanthanide complexes · Crystal structure · Aromatic carboxylic acids · Thermal analysis · Luminescence property

## Introduction

Lanthanide complexes had drew more and more attention on account of their attractive topology [1] and coordination modes, as well as their applications in luminescence [2], catalysis [3], biological medicine [4], single molecule magnet [5], physical chemistry [6], and thermochemistry [7]. Lanthanide ions were often used as functional metal centers because of their large atomic radius, high coordination number [8], and flexible coordination configuration [9]. At the same time, the 4f–4f transition in lanthanide ions could make lanthanide complexes emit light [10]. Still, the f–f electron laporte transition prohibition [11] leads to the

decrease of molar absorption coefficient [12], and finally weaken the light absorption of lanthanide ions. The results showed that the organic ligands containing nitrogen and oxygen could effectively transfer energy to lanthanide ions as antennas [13]. Carboxyl oxygen in oxygenated aromatic carboxylic acid ligands not only had strong affinity [14], but also its –COOH group could deproton to form various bridging modes such as a single tooth, double tooth, and triple tooth [15], so novel structures and frameworks could be constructed [16]. The auxiliary nitrogen-containing ligand not only had high thermal stability and strong luminescence [17], but also had a large  $\pi$  bond structure, which could improve the rigidity and stability of the complexes [18]. High color purity, long life, and stable luminescence intensity were the outstanding fluorescence characteristics of lanthanide complexes [19]. Therefore, lanthanide complexes had important practical significance in the field of luminescent materials. The thermal decomposition mechanism and thermal analysis kinetics of the complexes were studied, which provided an important reference for the synthesis of functional materials with certain thermal stability [20, 21]. TG–DTG–DSC and FTIR were the most important

✉ Jian-Jun Zhang  
jjzhang6@126.com

<sup>1</sup> Testing and Analysis Center, College of Chemistry & Material Science, Hebei Normal University, Shijiazhuang 050024, People's Republic of China

<sup>2</sup> Hebei Key Laboratory of Heterocyclic Compounds, College of Chemical Engineering & Material, Handan University, Handan 056005, People's Republic of China

and basic methods to analyze the thermal decomposition process of lanthanide complexes [22]. TG–DSC technology could detect the thermal decomposition products at different temperatures and determine the thermal decomposition mechanism. TG–DSC/FTIR could detect the main components of gas escaping during thermal decomposition at different temperatures [23].

Three new lanthanide complexes  $[\text{Ln}(2,4,6\text{-TMBA})_3(\text{terpy})(\text{H}_2\text{O})]\cdot\text{C}_2\text{H}_5\text{OH}\cdot\text{H}_2\text{O}$  ( $\text{Ln} = \text{Gd}(1)$ ,  $\text{Er}(2)$ ) and  $[\text{Tb}(2,4,6\text{-TMBA})_3(\text{terpy})(\text{H}_2\text{O})]\cdot\text{C}_2\text{H}_5\text{OH}(3)$  were synthesized with 2,4,6-trimethylbenzoic acid (2,4,6-TMBA) as acidic ligand, 2,2':6',2'-terpyridine (terpy) as neutral ligand and  $\text{Ln}(\text{NO}_3)_3\cdot 6\text{H}_2\text{O}$  as central ion. They were characterized by elemental analysis, infrared spectroscopy, and single-crystal X-ray diffraction. The thermal decomposition process of the complexes were determined by TG-DSC/FTIR, and the escaping gas was studied. Besides, the fluorescence properties and fluorescence lifetime of complex 3 was determined.

## Experimental

### Materials and reagents

The reagents and drugs selected in this experiment were of high purity and do not need further refinement.

### Experimental equipment and conditions

The contents of elements (C, H, and N) in the complexes were determined by Germany Elemental vario EL-III element analyzer. The single-crystal data were collected on the smart-1000 (Bruker AXS) single-crystal diffractometer with  $\text{Mo-K}\alpha$  monochromated graphite as the emission source, and the obtained structure was modified and improved by the SHELXS-97 program. Raman spectra were recorded by scanning 64 times with the BRUKER VERTEX-70 FTIR-RAMANII instrument under excitation power of 300 mW and liquid nitrogen cooling  $-\text{LnGaAs}$ . The TG–DTG–DSC

**Table 1** Elemental analysis data of complexes 1–3

Complexes	C/% (found)	H/% (found)	N/% (found)
1	56.09 (56.12)	4.72 (4.78)	4.36 (4.37)
2	55.57 (55.54)	4.79 (4.73)	4.28 (4.32)
3	59.67 (59.63)	5.56 (5.50)	4.50 (4.44)

and FTIR analysis of the complexes were measured by NETZSCH STA 449 F3 synchronous thermal analyzer and BRUKER TENSOR27 Fourier transform infrared spectrometer. They were all measured at a warming rate of  $10 \text{ K}\cdot\text{min}^{-1}$  under simulated atmospheric conditions. A 1.5 m transmission tube was needed to connect the infrared gas chamber with the thermal analyzer when measuring the escaping gas in the decomposition process. Among them, the diameter of the built-in PTFE tube in the transmission tube was 3 mm. In order to make the measured data more reliable, the temperature and sensitivity of the instrument were calibrated with Zn, In, Al, Au, Bi, and Sn standard samples before the experiment. The temperature of the transfer tube and the infrared gas chamber should be raised to 473.15 K before testing the sample and maintained at this temperature during sample testing. During sample measurement, an empty  $\text{Al}_2\text{O}_3$  crucible without a lid was used as a reference, and 6–7 mg samples were placed in another crucible. The fluorescence spectra and lifetime of solid complexes were determined by F5 fluorescence spectrometer at room temperature.

### Preparation of complexes 1–3

The acidic ligand 2,4,6-TMBA and neutral ligand terpy were dissolved in 7 mL of 95% ethanol in a molar ratio of 3:1. Stir and adjust pH to 5–7 with  $1 \text{ mol}\cdot\text{L}^{-1}$  NaOH. Drop the prepared ligand solution into the lanthanide nitrate aqueous solution. Stir for 6–8 h, and let stand for 12 h. Put the filtered mother liquor into the beaker and stand for 1–2 weeks to obtain the crystal.

**Table 2** IR and R spectra of complexes and ligands (values in  $\text{cm}^{-1}$ )

Ligands/complexes	$\nu_{\text{C=N}}$		$\delta_{\text{C-H}}$		$\nu_{\text{C=O}}$		$\nu_{\text{as}(\text{COO}^-)}$		$\nu_{\text{s}(\text{COO}^-)}$		$\nu_{(\text{Ln-O})}$		$\nu_{(\text{Ln-N})}$
	IR	R	IR	R	IR	R	IR	R	IR	R	IR	R	R
2,4,6-TMHBA					1675	1690							
terpy	1560	1471	838	761	835								
1	1538	1452	823	773	762		1542	1569	1447	1336	418	390	277
2	1542	1455	823	774	762		1542	1569	1449	1335	418	391	278
3	1539	1452	825	775	763		1541	1567	1447	1338	414	390	276

**Table 3** Crystal data and structure refinement of complexes 1–3

Complexes	1	2	3
Empirical formula	C <sub>47</sub> H <sub>54</sub> GdN <sub>3</sub> O <sub>9</sub>	C <sub>47</sub> H <sub>54</sub> ErN <sub>3</sub> O <sub>9</sub>	C <sub>47</sub> H <sub>52</sub> TbN <sub>3</sub> O <sub>8</sub>
Formula mass	962.18	972.19	945.84
Temperature/K	293(2)	293(2)	298(2)
Wavelength/Å	0.71073	0.71073	0.71073
Crystal system	Monoclinic	Monoclinic	Monoclinic
Space group	<i>P2(1)/c</i>	<i>P2(1)/c</i>	<i>P2(1)/c</i>
<i>a</i> /Å	13.9162(12)	13.8990(12)	14.2450(15)
<i>b</i> /Å	27.212(3)	27.234(2)	27.374(3)
<i>c</i> /Å	11.5958(11)	11.6060(11)	11.5443(12)
<i>α</i> /°	90	90	90
<i>β</i> /°	97.039(2)	97.148(2)	94.832(2)
<i>γ</i> /°	90	90	90
Volume/Å <sup>3</sup>	4358.1(7)	4359.0(7)	4485.7(8)
Z, Calculated density/Mg·m <sup>-3</sup>	4, 1.466	4, 1.481	4, 1.401
Absorption coefficient/mm <sup>-1</sup>	1.581	1.984	1.631
<i>F</i> <sub>(000)</sub>	1972	1988	1936
Crystal size/mm	0.42 × 0.06 × 0.03	0.27 × 0.09 × 0.06	0.14 × 0.05 × 0.03
Theta range for data collection/°	2.10 to 25.02	2.10 to 25.02	2.07 to 25.02
Limiting indices	− 16 ≤ <i>h</i> ≤ 16 − 29 ≤ <i>k</i> ≤ 32 − 13 ≤ <i>l</i> ≤ 13	− 16 ≤ <i>h</i> ≤ 15 − 27 ≤ <i>k</i> ≤ 32 − 13 ≤ <i>l</i> ≤ 13	− 16 ≤ <i>h</i> ≤ 16 0 ≤ <i>k</i> ≤ 32 0 ≤ <i>l</i> ≤ 13
Reflections collected/unique	21650/7657 [ <i>R</i> <sub>(int)</sub> = 0.0687]	21789/7691 [ <i>R</i> <sub>(int)</sub> = 0.0767]	7884/7884 [ <i>R</i> <sub>(int)</sub> = 0.0000]
Completeness to theta = 25.02°	99.5%	99.9%	99.6%
Max. and min. transmission	0.9541 and 0.5564	0.8902 and 0.6164	0.9527 and 0.8038
Data/restraints/parameters	7657/13/552	7691/73/541	7884/326/533
Goodness-of-fit on <i>F</i> <sup>2</sup>	1.083	1.089	1.035
Final <i>R</i> indices [ <i>I</i> > 2σ( <i>I</i> )]	<i>R</i> <sub>1</sub> = 0.0659 <i>wR</i> <sub>2</sub> = 0.1395	<i>R</i> <sub>1</sub> = 0.0536 <i>wR</i> <sub>2</sub> = 0.1006	<i>R</i> <sub>1</sub> = 0.1129 <i>wR</i> <sub>2</sub> = 0.1908
<i>R</i> indices (all data)	<i>R</i> <sub>1</sub> = 0.0948 <i>wR</i> <sub>2</sub> = 0.1512	<i>R</i> <sub>1</sub> = 0.0761 <i>wR</i> <sub>2</sub> = 0.1078	<i>R</i> <sub>1</sub> = 0.2735 <i>wR</i> <sub>2</sub> = 0.2284
Largest diff. peak and hole(e Å <sup>-3</sup> )	1.381 and − 3.451	1.092 and − 3.076	1.716 and − 1.645

**Table 4** Hydrogen bonding parameters of complexes 1, 2, and 3

D–H...A	d(D–H)/Å	d(H...A)/Å	<DHA/°	d(D...A)/Å
Complex 1				
O <sup>7</sup> –H <sup>7B</sup> ...O <sup>9</sup>	0.849	1.876	145.90	2.623
O <sup>7</sup> –H <sup>7C</sup> ...O <sup>6</sup>	0.845	1.965	144.80	2.700
Complex 2				
O <sup>7</sup> –H <sup>7B</sup> ...O <sup>9</sup>	0.850	1.888	146.20	2.637
O <sup>7</sup> –H <sup>7C</sup> ...O <sup>6</sup>	0.845	1.980	144.80	2.714
Complex 3				
O <sup>7</sup> –H <sup>7B</sup> ...O <sup>6</sup>	0.850	1.884	153.42	2.671
O <sup>7</sup> –H <sup>7C</sup> ...O <sup>8</sup>	0.850	2.110	132.39	2.755

## Results and discussion

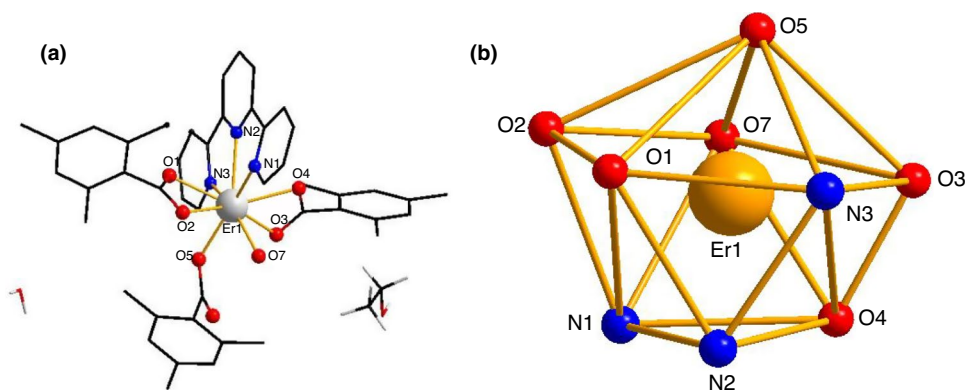
### Composition of complexes

Table 1 lists the content of element (C, H, and N) in the complexes, and the experimental value on the verge of the theoretical value. It showed that the complexes obtained in the experiment were relatively pure.

### Infrared and Raman spectra of complexes

To study the structure of the complexes more accurately, the Raman spectra complementary to the infrared spectra were measured at the same time [24]. Table 2 showed the infrared absorption data and Raman absorption data. The data in Table 2 showed that the acid ligand 2,4,6-TMBA had high activity at 1675 cm<sup>-1</sup> (IR) and 1690 cm<sup>-1</sup> (R)

**Fig. 1** **a** The crystal structure of complex 2, **b** The polyhedral model of  $\text{Er}^{3+}$  ion center



**Table 5** The shape calculation results of the central ions of complexes 1–3

Complexes	MFF-9	CSAPR-9	JCSAPR-9	TCTPR
Gd1	1.511	2.134	2.892	3.003
Er1	1.476	2.099	2.850	2.952
Tb1	1.685	2.126	2.805	3.215

*MFF-9* muffin, *CSAPR-9* spherical capped square antiprism, *JCSAPR-9* capped square antiprism J10, *TCTPR-9* spherical tri-capped trigonal prism

$\nu_{\text{C}=\text{O}}$  characteristic absorption band, but not found in the complexes. However, new characteristic absorption bands of  $\nu_{\text{as}(\text{COO}^-)}$  and  $\nu_{\text{s}(\text{COO}^-)}$  belonging to carboxylic acid anion were observed in the complexes. These characteristic absorption bands were located at  $1540\text{--}1542\text{ cm}^{-1}$  (IR),  $1567\text{--}1569\text{ cm}^{-1}$  (R),  $1447\text{--}1449\text{ cm}^{-1}$  (IR), and  $1335\text{--}1338\text{ cm}^{-1}$  (R), respectively. By comparing the spectral data of neutral ligand and complexes, it was found that the strong characteristic absorption bands of  $\nu_{\text{C}=\text{N}}$  ( $1538\text{--}1542\text{ cm}^{-1}$  (IR),  $1452\text{--}1455\text{ cm}^{-1}$  (R)) and  $\delta_{\text{C}-\text{H}}$  ( $823\text{--}825\text{ cm}^{-1}$  (IR),  $773\text{--}775\text{ cm}^{-1}$  (IR) and  $762\text{--}763\text{ cm}^{-1}$  (R)) after the formation of the complexes shifted. The characteristic absorption bands of Ln–O and Ln–N were noticed at  $414\text{--}419\text{ cm}^{-1}$  (IR),  $390\text{--}392\text{ cm}^{-1}$  (R) and  $276\text{--}278\text{ cm}^{-1}$  (R). Through the above analysis, it could be concluded that

the oxygen atom in the acidic ligand 2,4,6-TMBA and the nitrogen atom in the neutral ligand terpy coordinated with lanthanide ions. It was speculated that new products were formed [25, 26].

### Description of crystal structure

By analyzing the single crystal diffraction data in Table 3, it was observed that the crystal diffraction data of complexes 1–2 were relatively close, but they were different from that of complex 3. These three complexes could be segmented into two types. Therefore, the crystal structures of these two types were discussed in detail with complexes 2 and 3 as representatives. Table 4 lists the hydrogen bond parameters of the three complexes.

#### [Er(2,4,6-TMBA)<sub>3</sub>(terpy)(H<sub>2</sub>O)]·C<sub>2</sub>H<sub>5</sub>OH·H<sub>2</sub>O(2)

According to the crystal diffraction data in Table 2, complex 2 crystallizes in  $P2(1)/c$  space group of monoclinic system. As could be seen in Fig. 1a, it was a complex with a coordination number of nine composed of one Er(III) ion, three 2,4,6-TMBA, one terpy, one coordination water molecule, one free ethanol molecule, and one free water molecule. Six oxygen atoms were from 2,4,6-TMBA ligand and water, respectively, O1 and O2, O3 and O4 were coordinated by

**Table 6** The selected bond lengths of complexes 1–3 (values in Å)

Complex 1	Bond length/Å	Complex 2	Bond length/Å	Complex 3	Bond length/Å
Gd(1)–O(5)	2.226(6)	Er(1)–O(5)	2.229(4)	Tb(1)–O(5)	2.280(13)
Gd(1)–O(7)	2.310(6)	Er(1)–O(7)	2.302(4)	Tb(1)–O(7)	2.407(11)
Gd(1)–O(1)	2.383(6)	Er(1)–O(1)	2.382(5)	Tb(1)–O(3)	2.439(10)
Gd(1)–O(4)	2.395(6)	Er(1)–O(4)	2.387(5)	Tb(1)–O(2)	2.455(10)
Gd(1)–O(3)	2.437(6)	Er(1)–O(3)	2.439(5)	Tb(1)–N(3)	2.483(16)
Gd(1)–N(1)	2.477(7)	Er(1)–N(1)	2.474(6)	Tb(1)–O(1)	2.512(11)
Gd(1)–N(3)	2.496(7)	Er(1)–N(3)	2.493(5)	Tb(1)–N(1)	2.590(16)
Gd(1)–N(2)	2.499(6)	Er(1)–N(2)	2.498(5)	Tb(1)–N(2)	2.614(14)
Gd(1)–O(2)	2.580(6)	Er(1)–O(2)	2.582(5)	Tb(1)–O(4)	2.653(11)

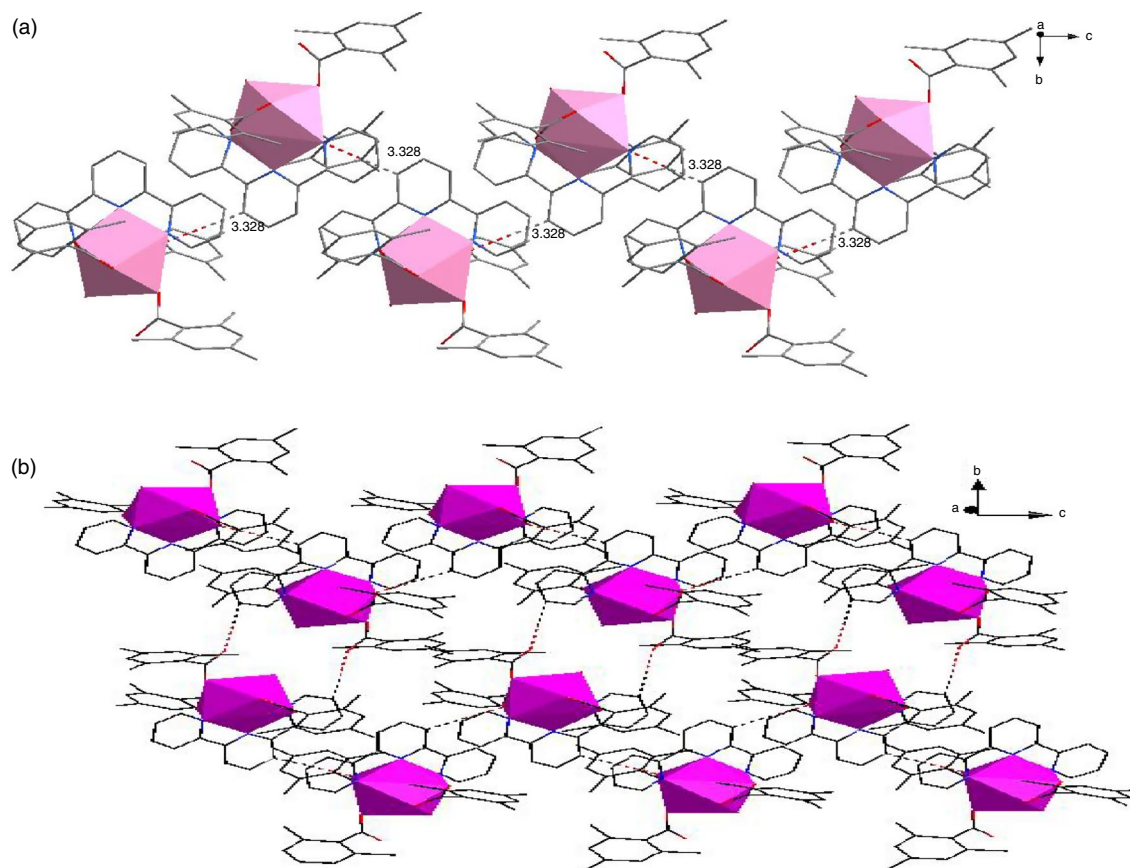
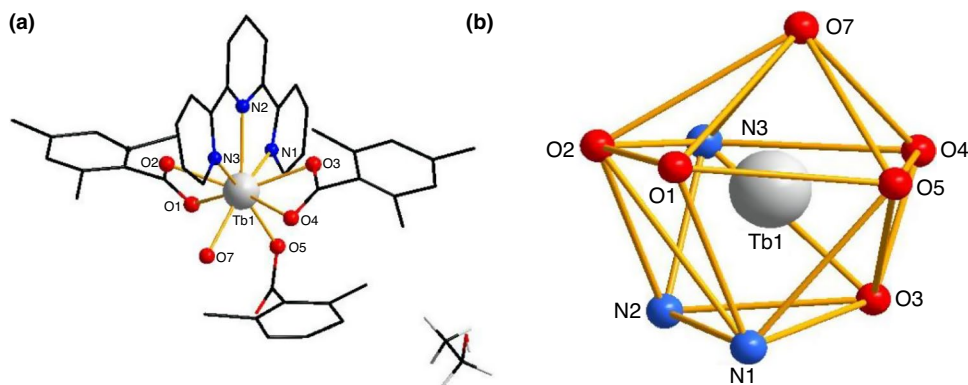


**Fig. 2** **a** The one-dimensional chains structure along the *c* axis of complex 2, **b** the two-dimensional sheet in about the *bc* plane

**Fig. 3** **a** The crystal structure of complex 3, **b** The polyhedral model of  $Tb^{3+}$  ion center



chelating bidentate, O5 was coordinated by monodentate, the other three nitrogen atoms were from terpy, and N1, N2 and N3 were coordinated by chelating tridentate. Import the crystal diffraction data into shape software [27], and calculated that the coordination environment of complex 2 was Muffin (Fig. 1b). The data were shown in Table 5.

By comparing the bond lengths of Er–N and Er–O in Table 6, it was found that the average bond length of Er–O (2.337 Å) was less than that of Er–N (2.483 Å). The main

reason was that oxygen had better coordination ability than nitrogen. It could be seen from Fig. 2 that because of the interaction of hydrogen bond, the complex forms a one-dimensional chain structure with C–H...O hydrogen bond distance of 3.328 Å in the *c* direction (Fig. 2a). The one-dimensional chain structure in the *c* direction forms a two-dimensional planar structure along the *bc* plane through the interaction of hydrogen bonds between ligands (Fig. 2b).



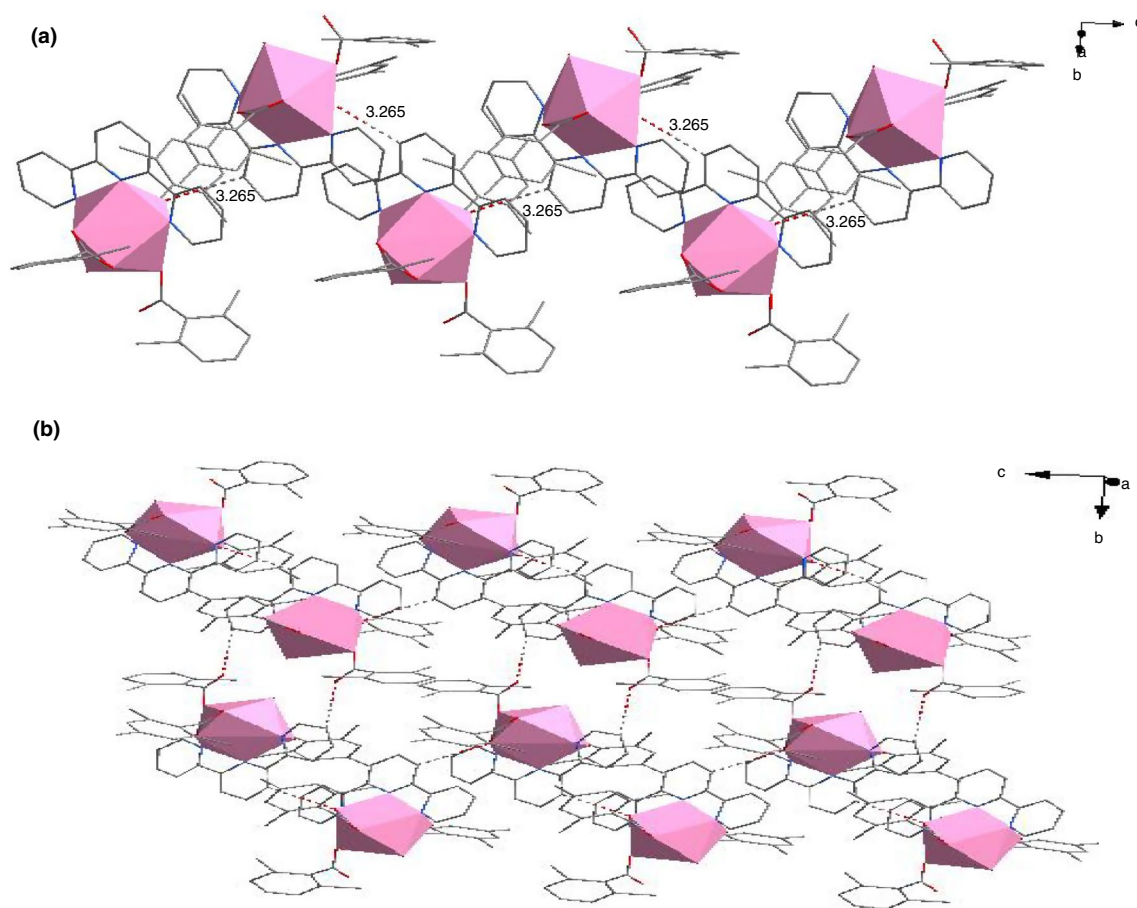


**Fig. 4** **a** The 1D chains structure along the *c* axis of complex 3, **b** the two-dimensional sheet in about the *bc* plane

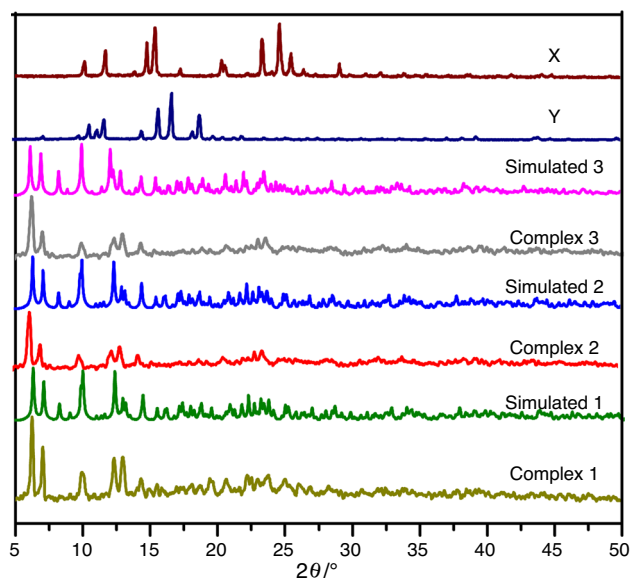


**Fig. 5** The experimental and simulated XRD patterns of complexes and the experimental XRD patterns of the ligands (X: 2,4,6-TMBA, Y: terpy)

Compared with the complex  $[\text{Er}(\text{2-Br-5-MOBA})_3(\text{terpy})(\text{H}_2\text{O})]$  (2-Br-5-MOBA = 2-bromine-5-methoxybenzoate; terpy = 2,2':6',2'-terpyridine) previously reported by Zhao qingqing [28], it was found that the title complexes and the reported complexes were mononuclear molecules, but the coordination number of the reported complex was eight, the coordination environment was a slightly distorted square anti-prismatic, and the coordination mode of its carboxylic acid ligand were chelating bidentate and monodentate. These were different from the title complexes. In addition, the title complexes also had free water and free ethanol. The reason for this difference may be that the carboxylic acid ligand of the title complexes does not contain halogen, and the carboxylic acid ligand in the reported complexes contains halogen (the interaction between halogen and halogen). Secondly, the carboxylic acid ligand in the reported complexes had two substituents at positions 2 and 4. In comparison, the carboxylic acid ligand of the target complexes had three substituents at positions 2, 4 and 6, and the substituents at positions 2 and 6 had large steric hindrance [29]. In conclusion, different carboxylic acid ligands may affect the coordination mode. That leads to different coordination structures.

**Table 7** The thermal analysis data of complexes 1 and 3

Complex	Steps	Temperature range/K	DTG $T_p$ /K	Mass loss rate/%		Probable expelled groups	Residue
				Found	Calcd		
1	I	321.15–412.15	355.25	7.16	8.53	2(H <sub>2</sub> O) + C <sub>2</sub> H <sub>5</sub> OH	[Gd(2,4,6-TMBA) <sub>3</sub> (terpy)]
	II	412.15–510.15	473.85	7.32	24.24	terpy	[Gd(2,4,6-TMBA) <sub>3</sub> ]
	III	510.15–571.15	549.45	18.27			
	IV	571.15–689.55	629.25	22.59	48.39	3(2,4,6-TMBA)	Gd <sub>2</sub> O <sub>3</sub>
	V	689.15–960.15	753.55	26.79	81.00		
2	I	321.15–414.15	346.15	7.37	8.43	2(H <sub>2</sub> O) + C <sub>2</sub> H <sub>5</sub> OH	[Er(2,4,6-TMBA) <sub>3</sub> (terpy)]
	II	414.15–510.15	476.05	6.46	23.99	terpy	[Er(2,4,6-TMBA) <sub>3</sub> ]
	III	510.15–577.15	544.55	18.03			
	IV	577.15–700.15	618.85	23.23	47.89	3(2,4,6-TMBA)	Er <sub>2</sub> O <sub>3</sub>
	V	700.15–974.15	767.65	24.36	78.81		
3	I	323.15–444.15	354.15	6.85	6.80	H <sub>2</sub> O + C <sub>2</sub> H <sub>5</sub> OH	[Tb(2,4,6-TMBA) <sub>3</sub> (terpy)]
	II	444.15–507.15	475.15	6.54	24.66	terpy	[Tb(2,4,6-TMBA) <sub>3</sub> ]
	III	507.15–575.15	549.65	18.21			
	IV	575.15–686.15	629.05	22.80	48.80	3(2,4,6-TMBA)	Tb <sub>4</sub> O <sub>7</sub>
	V	686.15–972.15	754.65	26.85	81.25		

### [Tb(2,4,6-TMBA)<sub>3</sub>(terpy)(H<sub>2</sub>O)]·C<sub>2</sub>H<sub>5</sub>OH(3)

Like complex 2, complex 3 also belongs to the monoclinic *P2(1)/c* space group. As could be seen from Fig. 3a, it was a complex with a coordination number of nine. Each mononuclear molecule comprises a Tb(III) ion, three acidic ligands 2,4,6-TMBA, and one neutral ligand terpy. The five oxygen atoms (O1–O5) from 2,4,6-TMBA were coordinated by chelating bidentate and monodentate, respectively, while the nitrogen atoms (N1–N3) from terpy were coordinated by chelating tridentate. According to shape software calculation (Table 5), the coordination environment of complex 3 was Muffin (Fig. 3b). At the same time, the data in Table 6 showed that the average bond length of Tb–N was longer than that of Tb–O. It could be observed from Table 6 that the average bond length of Er–O was longer than that of Tb–O, because the increased nuclear charge of 4f electrons was not completely blocked by 5s and 5p electrons, it was the phenomenon of “lanthanide contraction” [30]. Complex 3 forms a one-dimensional chain structure through C–H···O hydrogen bonding in the *c* direction (Fig. 4a). Meanwhile, these chain structures further form two-dimensional planar structures on the *bc* plane through hydrogen bonding between ligands (Fig. 4b).

[Tb<sub>2</sub>(2,4,6-TMBA)<sub>6</sub>(phen)<sub>2</sub> (2,4,6-TMBA = 2,4,6-trimethylbenzoate, phen = phenanthroline) was reported by Li et al. [29]. It belongs to a different crystal system with the title complexes. In the meantime, the coordination number,

coordination mode, and coordination environment were also different from those of the title complexes. In addition, the average bond length of Tb–N in the title complex was shorter than that in the reported complex, because the affinity of terpy ligand for Tb(III) ion was stronger than that of phen for Tb(III) ion. It also showed that the auxiliary ligand will also affect the coordination structure when forming the complexes.

### X-ray powder diffraction

To better prove the title complexes had high purity [31], the X-ray powder diffraction of the ligand and complexes were determined. Moreover, the simulated peak of the complexes were similar to the actual test peak in terms of peak position and number. However, from the powder diffraction patterns of complexes 2 and 3 (Fig. 5), it was found that the position and number of peaks were different, which showed that complexes 2 and 3 had different crystal structures. The peak positions and quantities of complexes 1 and 2 were similar, it indicates that complexes 1 and 2 were isomorphous.

### Thermal analysis

Thermal stability was an important parameter in material application. To better research the behavior of complexes with temperature, the mass loss and peak values of the complexes at different temperature ranges were measured

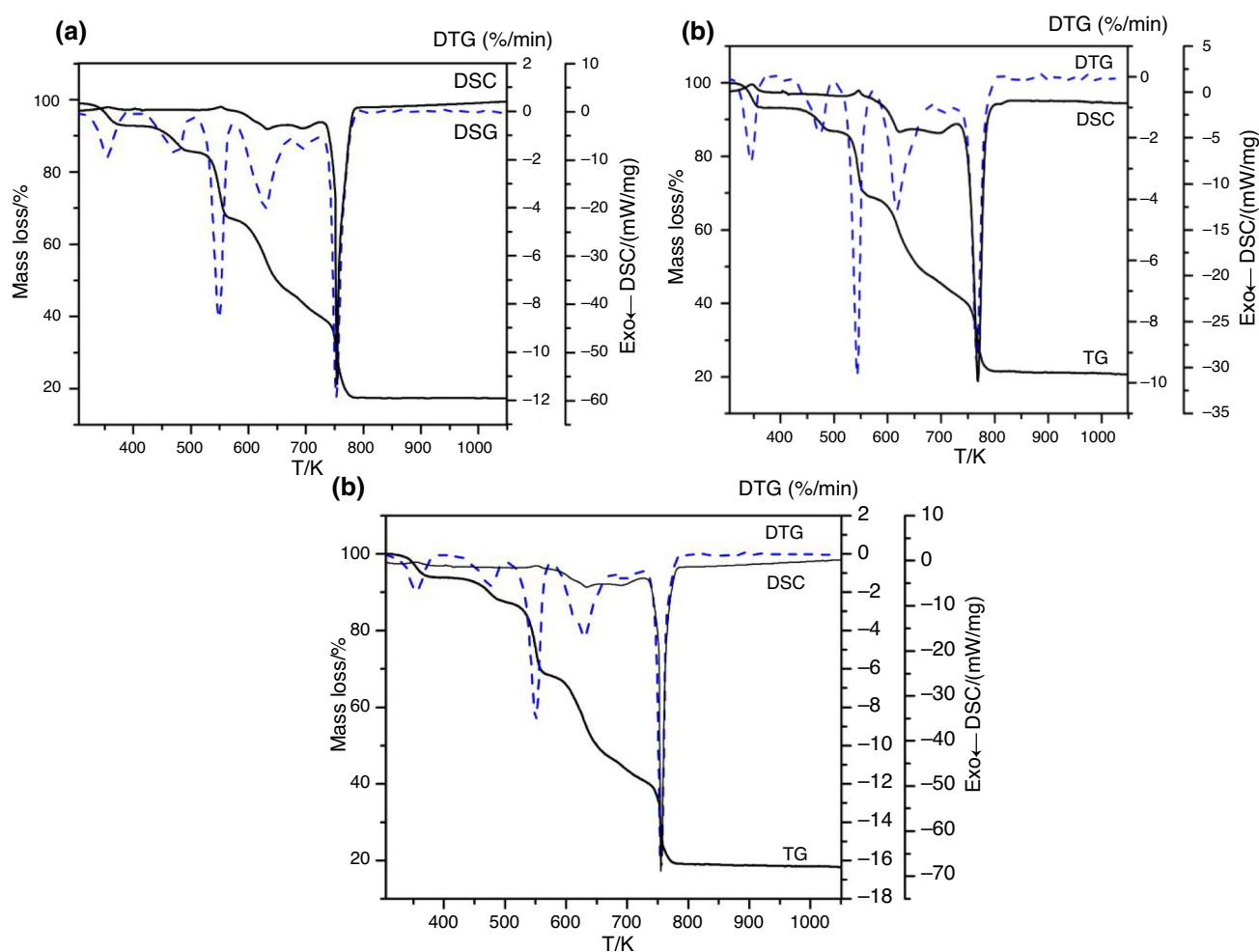


**Fig. 6** TG–DTG–DSC curves of complex 1 (a), complex 2 (b), and complex 3 (c)

(Table 7). The TG–DTG–DSC curves of complexes were shown in Fig. 6. Since complexes 1–3 were divided into two structural types by single crystal diffraction data, complexes 2 and 3 were taken as examples for detailed analysis.

It could be concluded that the decomposition process of complex 2 was divided into five steps. The decomposition of the first step starts at 321.15 K, ends at 414.15 K, the mass loss rate (7.37%) draw near the calculated theoretical value (8.43%) of losing one coordination water, one free water, and one free ethanol. Therefore, the first step could be attributed to the separation of water and ethanol molecules. The second step of decomposition began at 414.15 K and ended at 510.15 K. The mass loss rate was 5.82%, which correspond to the loss of some neutral ligands. The mass loss rate in the temperature range 510.15–577.15 K was 18.03%. The theoretical value of losing neutral ligands (23.99%) was just the total mass loss value of the second and third steps (23.85%), the mass lost in the third step was equivalent to the mass of the remaining neutral terpy ligands. There was also a weak endothermic peak on the DSC curve corresponding to the

third step. The mass losses of step 4 and step 5 were in the temperature range of 577.15–947.15 K, the total mass loss rate of these two steps (47.59%) approach the theoretical value of losing all acid ligands (47.89%). It was further suggested that the acid ligand was lost in these two steps. To sum up, after five steps of decomposition, the final residual mass was 21.19%, which was not much different from the theoretical residual mass of 19.69%. Therefore, the final product was  $\text{Er}_2\text{O}_3$ .

Combined with the analysis of the TG–DTG–DSC curve (Fig. 6c), the thermal decomposition process of complex 3 was split into five steps. The mass loss begins at 323.15 K. The mass loss rate (6.85%) was close to the calculated theoretical value of losing coordination water and free ethanol (6.80%). It means that the mass loss in the first step could be attributed to the breakdown of water and ethanol molecules. The second and third steps of decomposition took place between 414.15 and 577.15 K, the actual total mass loss rate (23.85%) of the second step (5.82%) and the third step (18.03%) differed little from the theoretical mass loss rate



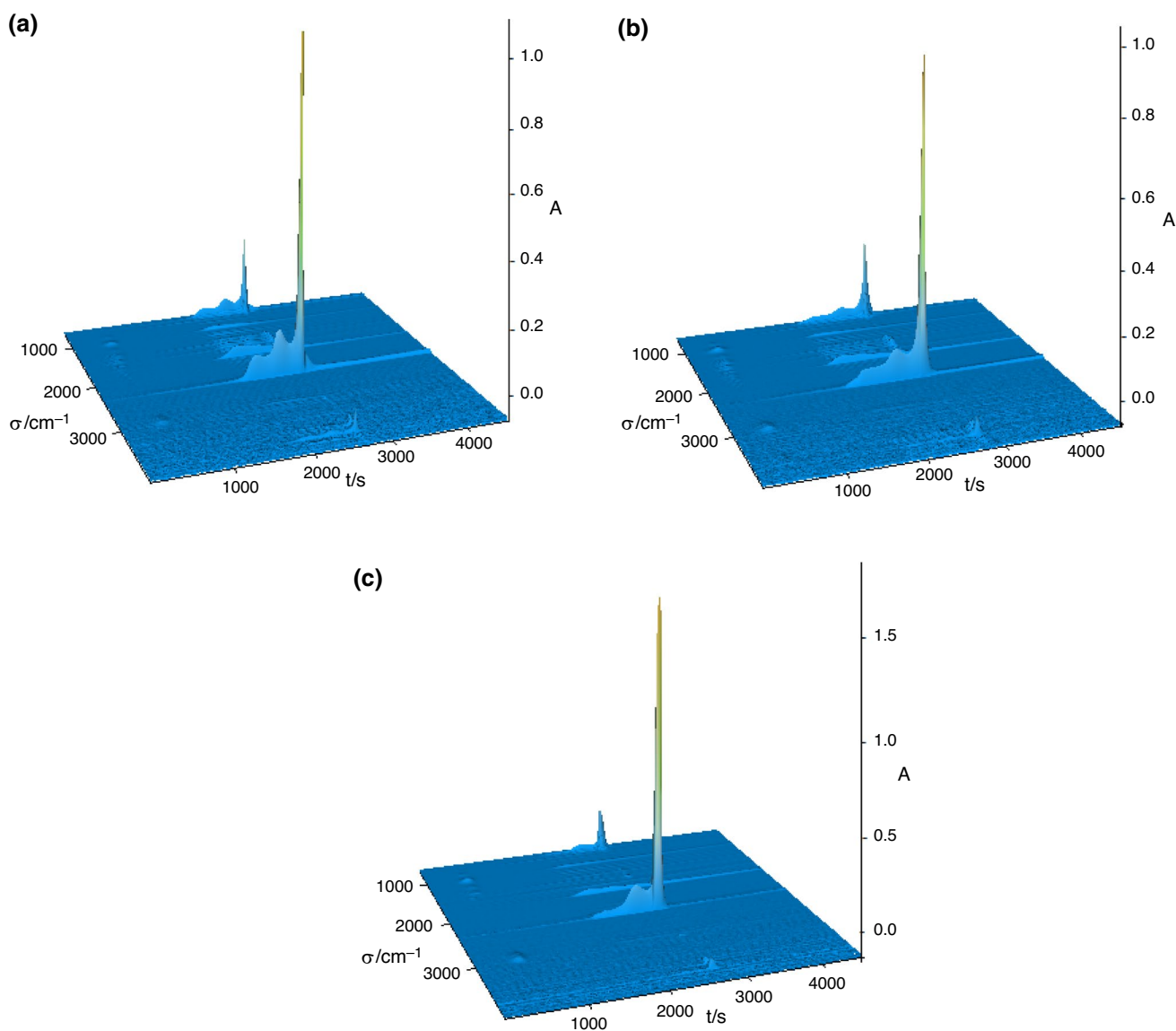


**Fig. 7** The 3D infrared stacking diagram of gas escaping during thermal decomposition of complexes: complex 1 (a), complex 2 (b), and complex 3 (c)

(23.99%) of the neutral ligand terpy. Therefore, these two steps could be classified as the decomposition of terpy. The decomposition of the fourth and fifth steps starts at 575.15 K and ends at 972.15 K. The total mass loss rate of these two steps (49.65%) approach the calculated theoretical value of loss of acidic ligand (48.8%). Finally, the entire mass loss (81.25%) was basically in accord with the theoretical mass loss (80.26%). The results showed that the final decomposition product was  $Tb_4O_7$ .

### Evolved gas analysis during thermal decomposition

To further determine the stability of the complexes in air and the gas products produced during thermal decomposition,

the three-dimensional infrared spectra of the gas escaping during thermal decomposition of the title complexes were measured by TG–DSC/FTIR (Fig. 7), and the two-dimensional infrared spectra at different temperatures were solved (Fig. 8). Because complexes 1 and 2 had the same crystal structures but was different from complex 3, we take complexes 2 and 3 as examples for detailed analysis.

The thermal decomposition process of complex 2 was segmented into five steps, and only four peaks appear in the three-dimensional infrared spectrum. This was mainly because the second step produces less gas and the pipeline of the instrument was long, so it was not detected. In the two-dimensional infrared spectrum of complex 2 (Fig. 8b), it was observed that there were characteristic

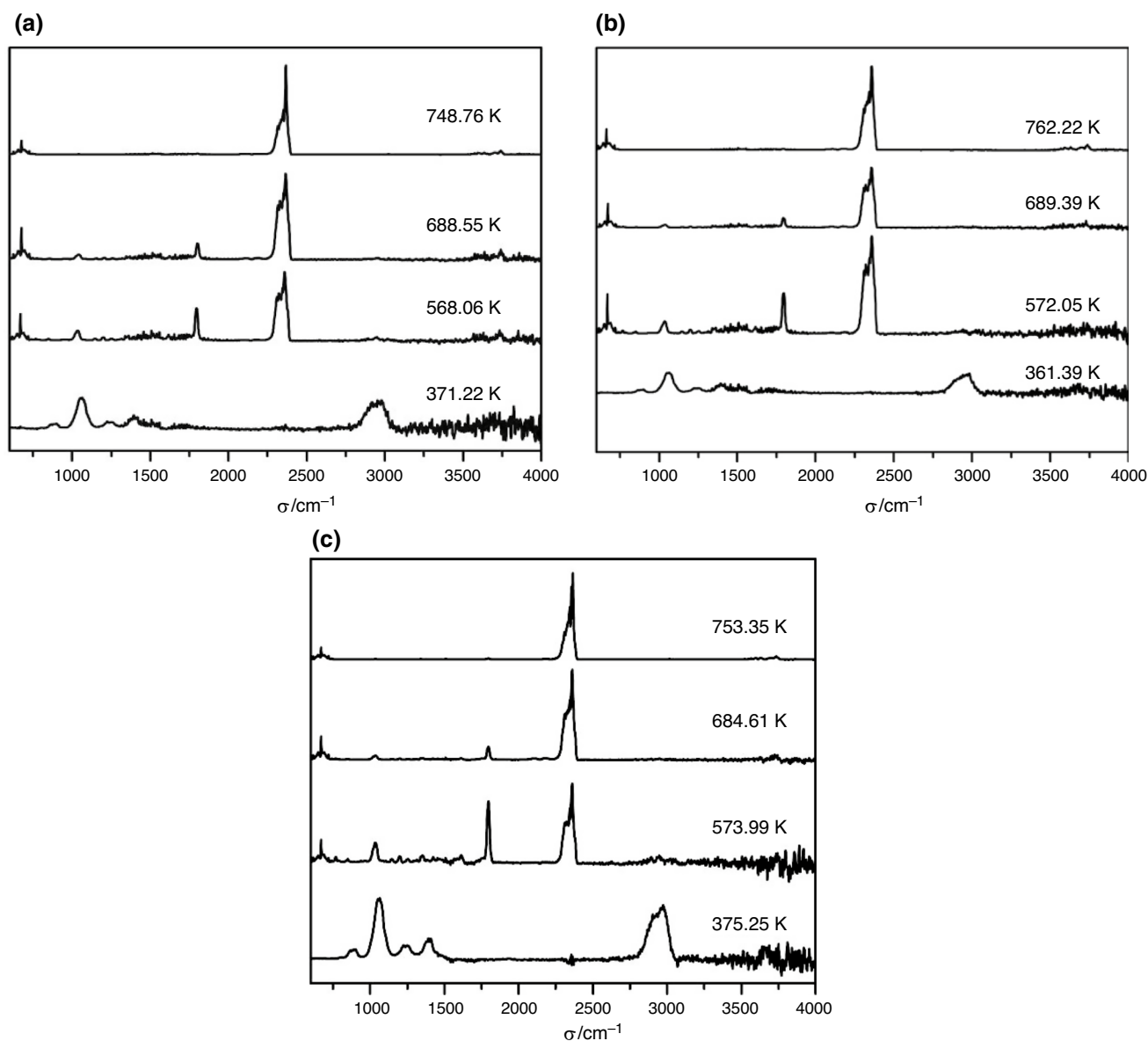


**Fig. 8** The 2D infrared spectra of complexes at different temperatures: complex 1 (a), complex 2 (b), and complex 3 (c)

absorption peaks of water molecule ( $3815\text{--}3832\text{ cm}^{-1}$ ) and ethanol molecule ( $3920\text{ cm}^{-1}$ ) at  $361.39\text{ K}$ , which was identify with the first step of the thermal decomposition process. It was further confirmed that the first step loss coordination water, free water, and ethanol molecules. The absorption bands of  $\nu_{\text{C-H}}$  ( $2935\text{--}3012\text{ cm}^{-1}$ ),  $\nu_{\text{C=C}}$  ( $1555\text{ cm}^{-1}$ ),  $\nu_{\text{C=N}}$  ( $1460\text{ cm}^{-1}$ ),  $\nu_{\text{C-N}}$  ( $1148\text{ cm}^{-1}$ ), and  $\gamma_{\text{C-H}}$  ( $670, 858, 1033\text{ cm}^{-1}$ ) organic molecular fragment belonging to terpy ligand were observed at  $572.05\text{ K}$ . It was further confirmed that the terpy was decomposed in this step. At the same time, a characteristic absorption peak of  $\nu_{\text{C=C}}$  ( $1520\text{ cm}^{-1}$ ) and  $\nu_{\text{C=O}}$  ( $1791\text{ cm}^{-1}$ ) belonging to 2,4,6-TMBA was observed at  $689.39\text{ K}$ . It showed that 2,4,6-TMBA was not completely decomposed in step

which was completely identified with the thermal decomposition process. Meanwhile, the characteristic peaks of  $\text{CO}_2$  and  $\text{H}_2\text{O}$  at  $2358\text{ cm}^{-1}$ ,  $663\text{ cm}^{-1}$ , and  $3735\text{ cm}^{-1}$  were observed at  $762.22\text{ K}$ . It means that 2,4,6-TMBA was completely decomposed in the fifth step. The final decomposition product was consistent with thermal decomposition, which was  $\text{Er}_2\text{O}_3$ .

Figure 8c was a two-dimensional spectrum of complex 3. The characteristic absorption peaks of water molecules were noticed at  $3750\text{--}3814\text{ cm}^{-1}$  and  $3820\text{ cm}^{-1}$ , respectively. It means that the first step of decomposition was the escape of coordinated water molecules and free ethanol molecules. Since the decomposition in the second step produces less gas and the pipeline channel was long, it was

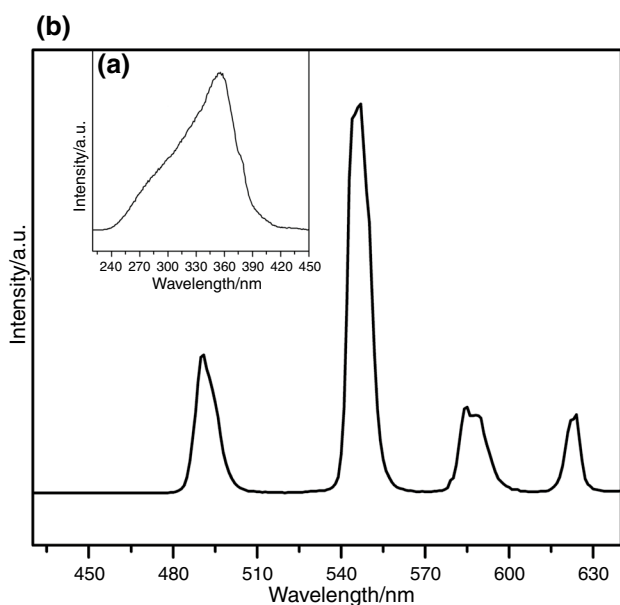


Fig. 9 Excitation (a) and emission (b) spectra of solid complex 3

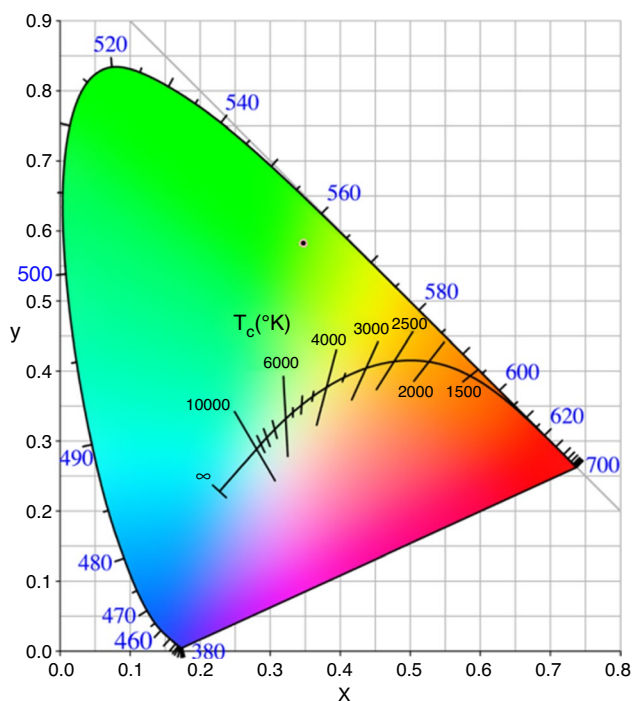


Fig. 10 Color coordinated diagram of complex 3

not detected. In the third step, the characteristic absorption peaks of organic molecular fragment  $\nu_{C-H}$ ,  $\nu_{C=C}$ ,  $\nu_{C=N}$ ,  $\nu_{C-N}$ , and  $\gamma_{C-H}$  were observed at 2953–3009  $\text{cm}^{-1}$ , 1570  $\text{cm}^{-1}$ , 1437  $\text{cm}^{-1}$ , 1141  $\text{cm}^{-1}$ , 849  $\text{cm}^{-1}$ , and 1032  $\text{cm}^{-1}$ , respectively. It was further proved that the

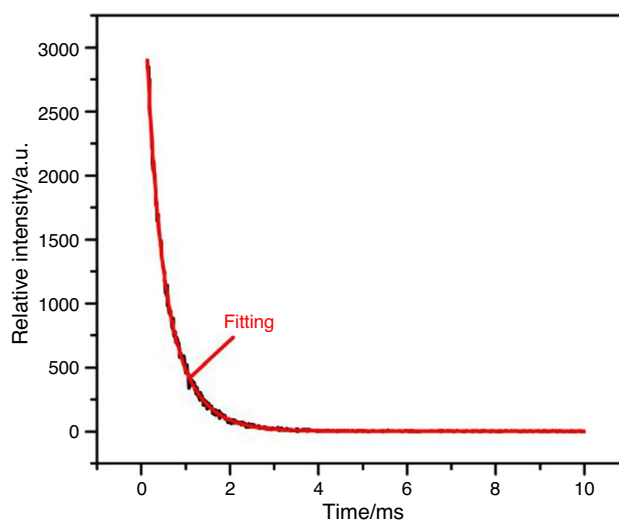


Fig. 11 Fluorescence life decay curve of complex 3

terpy was decomposed in this step. Moreover, the characteristic absorption peaks of  $\nu_{C=C}$  and  $\nu_{C=O}$  belonging to 2,4,6-TMBA ligands were observed at 1520  $\text{cm}^{-1}$  and 1793  $\text{cm}^{-1}$  in the fourth step. It indicates that the acidic ligands were not completely decomposed. The characteristic absorption peak of  $\text{CO}_2$  at 2353  $\text{cm}^{-1}$  in the fifth step was dominant. Meanwhile, the characteristic absorption peak of water molecules at 3735  $\text{cm}^{-1}$  was also observed. It indicates that the acidic ligand was completely decomposed in the fifth step, and the final product was  $\text{Tb}_4\text{O}_7$ . The above analysis corresponds to the thermal decomposition process.

### Luminescent properties

To better study the luminescent properties of complexes, the fluorescence spectra and fluorescence lifetime of solid complex 3 was measured. As could be seen from the excitation spectrum in Fig. 9a, there was a strong excitation wide peak in the range of 220–450 nm, which was mainly the absorption peak generated by electron transfer from the ligand to the central ion [32], and the intensity of the peak indicates that the energy transfer from the carboxylic acid ligand to the central ion was effective. The emission spectrum with 355 nm as the excitation wavelength was measured within limits 430–640 nm (Fig. 9b). The four characteristic transitions of Tb(III) ions could be observed. The transition intensity of  ${}^5\text{D}_4\text{--}{}^7\text{F}_5$  at 545 nm was greater than that of  ${}^5\text{D}_4\text{--}{}^7\text{F}_6$  (490 nm),  ${}^5\text{D}_4\text{--}{}^7\text{F}_4$  (590 nm), and  ${}^5\text{D}_4\text{--}{}^7\text{F}_3$  (620 nm), this could also explain the intense green glow of complex 3 under ultraviolet lamps [33]. At the same time, the emission spectrum data of complex 3 was substituted into the color coordinated (0.3475, 0.5824) calculated by the color coordinated software, and the black

dot was marked in the color coordinated diagram (Fig. 10). It was further showed that complex 3 emits strong green light.

Another parameter characterizing the luminescence properties of fluorescent materials was the fluorescence lifetime (Fig. 11). Therefore, the fluorescence lifetime decay curve of solid complex 3 at the best emission wavelength was collected. The fluorescence lifetime data of the complex was fitted by double exponential function equation:  $I(t) = B_1 \cdot \exp(-t/\tau_1) + B_2 \cdot \exp(-t/\tau_2)$ , and then the fitting parameters  $B_1$  and  $B_2$  and attenuation time  $\tau_1$  and  $\tau_2$  were substituted into formula  $\tau = (B_1\tau_1^2 + B_2\tau_2^2)/(B_1\tau_1 + B_2\tau_2)$ . It was calculated that the fluorescence of complex 3 was 0.637 ms.

## Conclusions

Three new mononuclear lanthanide complexes [Ln(2,4,6-TMBA)<sub>3</sub>(terpy)(H<sub>2</sub>O)]·C<sub>2</sub>H<sub>5</sub>OH·H<sub>2</sub>O (Ln = Gd(1), Er(2)) and [Tb(2,4,6-TMBA)<sub>3</sub>(terpy)(H<sub>2</sub>O)]·C<sub>2</sub>H<sub>5</sub>OH (3) were synthesized. Single-crystal X-ray diffraction showed that the coordination number of the three complexes were nine, the coordination environment was muffin, and they all form one-dimensional chain and 2D planar structures through C–H⋯O bonds. The difference was that complexes 1 and 2 had both free water molecules and free ethanol molecules, while complex 3 had only free ethanol molecules. The structure of the complexes were further determined by infrared and Raman spectra. The purity of the title complexes were proved to be high by elemental analysis and X-ray powder diffraction. At the same time, the thermal decomposition results showed that free molecules and coordination water were easier to decompose than ligands, while acidic ligands always begin to decompose after the loss of neutral ligands, and the last remaining product was metal oxides. The solid-state fluorescence test of complex 3 showed that terbium complex had characteristic green fluorescence, and its fluorescence lifetime was 0.637 ms. Therefore, it had broad application prospects in the field of luminescent materials.

## Supplementary data

The number of two complexes (CCDC 2110461 (1), CCDC 2110459 (2), CCDC 2110464 (3)) contain the supplementary crystallographic data for this paper. These data could be obtained free of charge from the Cambridge Crystallographic Data Centre via [www.ccdc.cam.ac.uk/data\\_request/cif](http://www.ccdc.cam.ac.uk/data_request/cif).

**Acknowledgements** The research work was supported by the National Natural Science Foundation of China (No. 21803016).

## References

- Chen Y, Liu SS, Gao R, Wang Y, Zhang WJ, Ju ZH. Synthesis, structures and luminescence of two lanthanide coordination polymers based on 2,4-pyridinedicarboxylic acid. *J Solid State Chem.* 2019;279:120931.
- You LX, Hao JH, Qi D, Xie SY, Wang SJ, Xiong G, Dragutan I, Dragutan V, Ding F, Sun YG. Lanthanide coordination polymers containing 1,3-bis(carboxymethyl) imidazolium as organic ligand: crystal structure and luminescent properties. *Inorg Chim Acta.* 2019;497:119075.
- Bernini MC, Gomez GE, Brusau EV, Narda GE. Reviewing rare earth succinate frameworks from the reticular chemistry point of view: structures, nets, catalytic and photoluminescence applications. *Isr J Chem.* 2018;58:1044–61.
- Zapała L, Kosińska M, Woźnicka E, Byczyński Ł, Ciszkowicz E, Lecka-Szlachta K, Zapała W, Chutkowski M. Comparison of spectral and thermal properties and antibacterial activity of new binary and ternary complexes of Sm(III), Eu(III) and Gd(III) ions with N-phenylanthranilic acid and 1,10-phenanthroline. *Thermochim Acta.* 2019;671:134–48.
- Wu Y, Xia CC, Wang XY. Syntheses, structures and magnetic properties of a series of lanthanide complexes with reduced nitronyl nitroxide radical ligands. *Inorg Chim Acta.* 2021;520:120308.
- Lu YL, Ma Y, Sun LZ, Kuang XN, Xin XL, Han HL, Liu M, Li ZF, Jin QH. 1D lanthanide coordination polymers containing biphosphonate ligand: synthesis, structures and luminescence properties. *Inorg Chem Commun.* 2020;118:108045.
- Zhou MX, Ren N, Zhang JJ. Crystal structure, thermal decomposition mechanism and properties of lanthanide supramolecular complexes based on 2,4,6-trimethylbenzoic acid and 5,5'-dimethyl-2,2'-bipyridine. *Acta Phys Chim Sin.* 2021;37:2004071.
- Cao FY, Huang MP, Gao HL, Zhao XL, Han J, Chen XD. Lanthanide complexes of anthraquinone-1,8-disulfonate: syntheses, structures and catalytic studies. *Inorg Chem Commun.* 2021;130:108682.
- Lu YB, Wang SH, Zhu SD, Zhuo YQ, Lin XL, Yang GM, Xie YR. The syntheses, structures, magnetic and luminescent properties of five new lanthanide(III) complexes based on tetrazole 1-acetic ligand. *Inorg Chem Commun.* 2020;111:107667.
- Bai C, Fu XY, Hu HM, He S, Wang X, Xue GL. Construction of visible luminescent lanthanide coordination compounds with different stacking modes based on a carboxylate substituted terpyridyl derivative ligand. *Inorg Chim Acta.* 2020;506:119550.
- Yuan G, Zhang C, Shao KZ, Hao XR, Zhou WL, Wang FC, Su ZM. A series of lanthanide coordination polymers based on flexible bis-(imidazole-4,5-dicarboxylate) ligand: syntheses, structures and fluorescent properties. *Inorg Chem Commun.* 2019;99:126–30.
- Mara D, Artizzu F, Laforce B, Vincze L, Van Hecke K, Van Deun R, Kaczmarek AM. Novel tetrakis lanthanide β-diketonate complexes: structural study, luminescence properties and temperature sensing. *J Lumin.* 2019;213:343–55.
- Smirnova KS, Ivanova EA, Sukhikh TS, Pozdnyakov IP, Dotsenko VV, Lider EV. Luminescent properties of Ln(III) complexes with

- 2-[(phenylamino)methylene]-5,5-dimethyl-cyclohexane-1,3-dione as an antenna. *Inorg Chim Acta*. 2021;525:120490.
14. Du DD, Ren N, Zhang JJ. Syntheses, crystal structures, thermodynamic and fluorescent properties of dinuclear lanthanide complexes constructed with 2-fluorobenzoic acid and 5,5'-dimethyl-2,2'-bipyridine. *J Therm Anal Calorim*. 2022;147:2527–36.
  15. Zhang WQ, Zhang RF, Zhang QF, Zhang SL, Ru J, Li QL, Ma CL. Four novel lanthanide(III) coordination complexes based on 3,4,5-trifluorobenzeneseleninic acid. *J Solid State Chem*. 2019;270:360–5.
  16. Wang PP, Chen WL, Xia J. Synthesis, structures, and properties of lanthanide complexes with pyrimidine-2-carboxylic acid. *Z Anorg Allg Chem*. 2017;643:1752–8.
  17. Wang CY, Kang J, Zhang XQ, Zhao YL, Chu HB. Crystal structures and luminescence properties of lanthanide complexes with 4-bromobenzoate and nitrogen heterocyclic ligands. *J Lumin*. 2019;215:116638.
  18. Kot K, Oczko G, Puchalska M, Starynowicz P. Structural and spectroscopic studies of heavy lanthanide complexes with o-phenanthroline and isothiocyanate. *Polyhedron*. 2019;173:114119.
  19. Gou J, Yang QQ, Li SY, Zhao LH, Gao HL, Cui JZ. [Ln<sub>4</sub>] complexes based on 8-hydroxylquinoline-schiff base: synthesis, crystal structure and near-infrared emission. *Polyhedron*. 2021;201:115165.
  20. Wang JJ, Zhang JJ. Thermal analysis kinetics and thermokinetics. *Acta Phys Chim Sin*. 2020;36(6):1909020.
  21. Ren N, Wang F, Zhang JJ, Zheng XF. Progress in thermal analysis kinetics. *Acta Phys Chim Sin*. 2020;36:1905062.
  22. Du DD, Ren N, Zhang JJ. A series of lanthanide complexes with 2-fluorobenzoic acid and 5,5'-dimethyl-2,2'-bipyridine: synthesis, supramolecular structures, spectroscopy and thermal behaviour. *J Solid State Chem*. 2021;300:122198.
  23. Li YY, Ren N, He SM, Zhang JJ. Supramolecular structures, thermal decomposition mechanism and heat capacity of the novel binuclear Tb(III) and Dy(III) complexes with 2,3 dimethoxybenzoic acid and 5,5'-dimethyl-2,2'-bipyridine. *J Therm Anal Calorim*. 2020;140:2435–45.
  24. He SM, Sun SJ, Zheng JR, Zhang JJ. Molecular spectrum of lanthanide complexes with 2,3-dichlorobenzoic acid and 2,2-bipyridine. *Spectrochim Acta Part A*. 2014;123:211–5.
  25. Di YQ, Cui XW, Liu YL, Zhou CS, Ren YL, Di YY, Yang X. Crystal structure, optical properties, and antibacterial activity of rare earth complexes with designed 2-carbonyl propionic acid-4-nitro benzoyl hydrazone. *Polyhedron*. 2019;171:571–7.
  26. Peewasan K, Merkel MP, Fuhr O, Powell AK. A designed and potentially decadentate ligand for use in lanthanide(III) catalysed biomass transformations: targeting diastereoselective trans-4,5-diaminocyclopentenone derivatives. *Dalton Trans*. 2020;49:2331–6.
  27. Madanhire T, Davids H, Pereira MC, Hosten EC, Abrahams Ar. Synthesis, characterisation and anticancer activity screening of lanthanide(III) acetate complexes with benzohydrazone and nicotinicohydrazone ligands. *Polyhedron*. 2020;184:114560.
  28. Zhao QQ, Ren N, Zhang JJ. Syntheses, crystal structures, luminescence and thermal properties of three lanthanide complexes with 2-bromine-5-methoxybenzoate and 2,2':6',2''-terpyridine. *Polyhedron*. 2018;144:1–5.
  29. Li DP, Feng YL, Chen ZM, Kuang DZ, Zhang CH, Yang YQ, Li W. Synthesis, crystal structure of a binuclear terbium complex with 2,4,6-trimethylbenzoic acid and 1,10-phenanthroline. *Chinese J Inorg Chem*. 2006;22(11):2097–100.
  30. Łyszczek R, Rusinek I, Sienkiewicz-Gromiuk J, Iwan M, Pavlyuk O. 3-D lanthanide coordination polymers with the flexible 1,3-phenylenediacetate linker: spectroscopic, structural and thermal investigations. *Polyhedron*. 2019;159:93–101.
  31. Fang WH, Yang GY. A series of lanthanide coordination polymers constructed from 4-pyridin-4-ylbenzoate. *Chem J Chin Univ*. 2015;31:187–91.
  32. Shang Q, Li Y, Yang EC, Zhao XJ. Three isostructural 4-sulphophthalate-based lanthanide complexes: syntheses, crystal structures, and luminescent properties. *Z Anorg Allg Chem*. 2015;641:2515–9.
  33. Zhao XQ, Zhang FH, Liu YJ, Zhao TH, Zhao HY, Xiang S, Li YC. A series of luminescent Ln(III)-based coordination polymers: syntheses, structures and luminescent properties. *Inorg Chim Acta*. 2020;504:119459.

**Publisher's Note** Springer Nature remains neutral with regard to jurisdictional claims in published maps and institutional affiliations.